Electronic Supplementary Information

Axially Rotating (Pt-salphen)$_2$ Phosphorescent Coordination Frameworks

Zhengqing Guo, Wah-Leung Tong and Michael C. W Chan*

Department of Biology and Chemistry, City University of Hong Kong, Tat Chee Avenue, Kowloon, Hong Kong, China. Email: mcwchan@cityu.edu.hk

Experimental details and characterization data for **1**–**4** and precursors; UV-vis and emission (298 and 77 K fluid and solid-state) data and spectra for **1** and **2**; description of molecular modeling for **1**; photograph showing colorimetric response and competition experiments showing ratiometric emission response for **1** to metal ions in CH_3CN; Job's plot and curve fittings for Pb^{2+} binding; ESI-MS of [**1** + Pb]$^{2+}$ using declustering potential of 50 V in CH_3CN; NMR experiments; emission changes of **1**–**4** with Pb^{2+}.

Experimental Section

General Considerations

Solvents for syntheses (analytical grade) were used without further purification and all metalation reactions were performed under a nitrogen atmosphere. Solvents for photophysical measurements were purified according to conventional methods. ^{1}H NMR spectra were obtained on Bruker DRX 300 and 400 FT-NMR spectrometers (ppm) using Me_4Si as internal standard. ESI mass spectra were measured on a Perkin-Elmer SCIEX API 365 mass spectrometer. IR spectra were recorded on a Perkin-Elmer 1600 series FT-IR spectrophotometer. Elemental analyses were performed on an Elementar Analysensysteme GmbH Vario EL elemental analyzer. UV-vis absorption spectra were obtained on an Agilent 8453 diode array spectrophotometer.

Steady-state emission spectra were recorded on a SPEX FluoroLog 3-TCSPC spectrophotometer equipped with a Hamamatsu R928 PMT detector, and emission lifetime measurements were conducted using NanoLed sources in the fast MCS mode and checked using the TCSPC mode. Sample and standard solutions were degassed with at least three freeze-pump-thaw cycles. Low-temperature (77 K) emission spectra for glasses and solid-state samples were recorded in 5-mm diameter quartz tubes which were placed in a liquid nitrogen Dewar equipped with quartz windows. The emission quantum yield was measured[1] by using $[Ru(bpy)_3](PF_6)_2$ in degassed acetonitrile as the standard ($\Phi_r = 0.062$) and calculated by: $\Phi_s = \Phi_r(B_r/B_s)(n_s/n_r)^2(D_s/D_r)$, where the subscripts s and r refer to sample and reference standard solution respectively, n is the refractive index of the solvents, D is the integrated intensity, and Φ is the luminescence quantum yield. The quantity B is calculated by the equation: $B = 1 - 10^{-AL}$; where A is the absorbance at the excitation wavelength and L is the optical path length. Errors for λ (± 1 nm), τ (± 10 %), and Φ (± 10 %) are estimated. Solutions of Pt(II) complexes and metal perchlorate salts were prepared in CH_3CN (spectroscopic grade). Absorption and emission titrations were carried out in a quartz cuvette by addition of small volumes of metal ion solutions (5×10^{-3} M) to the Pt(II) complex (10^{-5} M).

Synthetic Methods

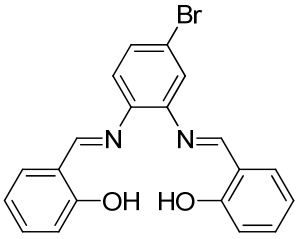

L1: A solution of salicylaldehyde (2.38 g, 7.95 mmol) and 4-bromo-1,2-diamino-benzene (1.82 g, 9.7 mmol) in EtOH (60 mL) was stirred at room temperature for 12 h. The yellow solid was collected by filtration and crystallized from EtOH to give orange needle crystals (2.52 g, 6.38 mmol) in 66% yield. ^{1}H NMR ($CDCl_3$, 300 MHz): δ 12.87 (s, 1H), 12.76 (s, 1H), 8.62 (s, 2H), 7.48-7.39 (m, 6H), 7.13 (d, J = 7.8 Hz, 1H), 7.05 (d, J = 8.1 Hz, 2H), 6.96-6.92 (m, 2H) ppm. IR (KBr, cm^{-1}): 3442, 2954, 2917, 2850, 1735, 1610, 1577, 1474, 1277, 1151.

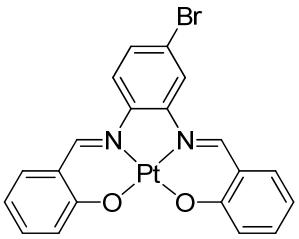

L2: K_2PtCl_4 (72 mg, 0.17 mmol), **L1** (69 mg, 0.17 mmol) and K_2CO_3 (72 mg, 0.52 mmol) were dissolved in degassed DMSO (10 mL), and the mixture was stirred at 75 ^{o}C for 12 h. The red solution was diluted with CH_2Cl_2 (50 mL) and H_2O (20 mL), and the aqueous phase was extracted with CH_2Cl_2 (3 × 10 mL). The combined organic phase was washed by brine (2 × 10 mL), dried over anhydrous Na_2SO_4 and concentrated *in vacuo*. The dark red solid was further dissolved with CH_2Cl_2 (10 mL), and Et_2O (50 mL) was added. The resultant red precipitate (55 mg, 0.09 mmol) was collected by centrifugation in 54% yield. ^{1}H NMR ($CDCl_3$, 300 MHz): δ 8.70 (s, 1H), 8.67 (s, 1H), 8.02 (s, 1H), 7.80 (d, J = 8.9 Hz, 1H), 7.61-7.52 (m, 3H), 7.50-7.39 (m, 2H), 7.35 (dd, J = 8.7, 2.8 Hz, 2H), 6.77 (t, J = 7.8 Hz, 1H), 6.73 (t, J = 7.2 Hz, 1H) ppm.

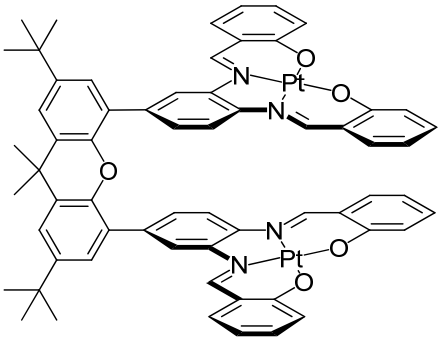

1: 2,7-Di-*tert*-butyl-9,9-dimethylxanthene-4,5-diboronic acid[2] (17 mg, 0.04 mmol), **L2** (52 mg, 0.08 mmol), $Pd(PPh_3)_4$ (5 mg, 0.004 mmol) and potassium carbonate (22 mg, 0.16 mmol) was charged in a two-necked flask under nitrogen. DMF (10 mL) was degassed *via* three freeze-pump-thaw cycles and added to the mixture, which was stirred at 75 °C for 48 h. The solvent was removed and the residue dissolved in CH_2Cl_2 (30 mL). After washing with water (3 × 30 mL), the organic phase was dried over anhydrous Na_2SO_4 and concentrated *in vacuo*. The crude product was dissolved in CH_2Cl_2 (5 mL), then addition of Et_2O (20 mL) led to a red solid. This procedure was repeated several times, and recrystallization in CH_2Cl_2/Et_2O gave a red precipitate (20 mg, 44 %). ^{1}H NMR (CD_2Cl_2, 400 MHz): δ 7.89 (s, 2H), 7.77 (s, 2H, *H*-C=N), 7.69 (s, 2H, *H*-C=N), 7.69-7.56 (m, 6H), 7.40 (d, J = 7.2 Hz, 2H), 7.34 (d, J = 2.0 Hz, 2H), 7.30 (d, J = 8.0 Hz, 2H), 7.24-7.21 (m, 4H), 7.12 (d, J = 8.8 Hz, 2H), 6.89 (d, J = 8.8 Hz, 2H), 6.79 (t, J = 7.2 Hz, 2H), 6.75 (t, J = 8.0 Hz, 2H) ppm. ESI-MS (*m*/*z*): 1337 $[M + H]^+$. IR (KBr, cm^{-1}): 2955, 2917, 2850, 1736, 1609, 1525, 1464 and 1180. Found: C, 56.49; H, 4.09; N, 4.44. Calc. for $C_{63}H_{54}N_4O_5Pt_2$: C, 56.58; H, 4.07; N 4.19.

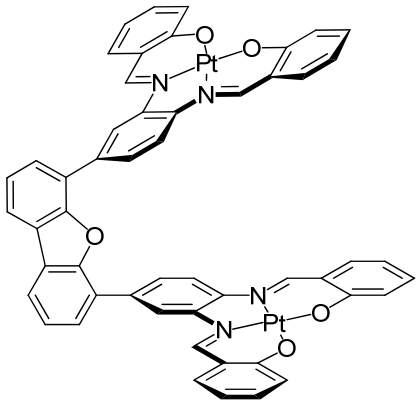

2: Dibenzofuranyl-4,6-bisboronic acid[3] (22 mg, 0.09 mmol), **L2** (100 mg, 0.17 mmol), $Pd(PPh_3)_4$ (4 mg, 0.003 mmol) and potassium carbonate (35 mg, 0.26 mmol) were charged in a two-necked flask under nitrogen. DMF (10 mL) was degassed *via* three freeze-pump-thaw cycles and added to the mixture, which was stirred at 75 °C for 48 h. The solvent was then

removed and the residue dissolved in CH_2Cl_2 (30 mL). After washing with water (3 × 30 mL), the organic phase was dried over anhydrous Na_2SO_4 and concentrated *in vacuo*. The crude product was dissolved in CH_2Cl_2 (5 mL), then addition of Et_2O (20 mL) led to a red solid. This procedure was repeated several times, and recrystallization in CH_2Cl_2/Et_2O gave a red precipitate (19 mg, 19 %). ^{1}H NMR (CD_2Cl_2, 400 MHz): δ 8.91 (s, 2H), 8.48 (s, 2H, *H*-C=N), 8.17 (s, 2H, *H*-C=N), 8.12 (d, J = 7.6 Hz, 2H), 8.00 (d, J = 9.2 Hz, 2H), 7.86 (d, J = 7.6 Hz, 2H), 7.80 (d, J = 9.2 Hz, 2H), 7.61-7.57 (m, 4H), 7.51 (d, J = 8.0 Hz, 2H), 7.31 (d, J = 9.2 Hz, 2H), 6.81-6.76 (m, 4H), 6.69 (t, J = 7.2, 6.4 Hz, 2H), 6.53 (d, J = 8.0 Hz, 2H), 6.28 (t, J = 7.6, 6.8 Hz, 2H) ppm. ESI-MS (*m*/*z*): 1183 $[M + H]^+$. IR (KBr, cm^{-1}): 2955, 2917, 2850, 1737, 1608, 1525, 1463 and 1181. Found: C, 53.00; H, 2.95; N, 5.08. Calc. for $C_{52}H_{32}N_4O_5Pt_2$: C, 52.79; H, 2.73; N 4.74.

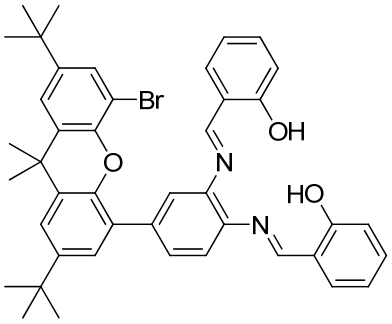

L3: Modifications of a published procedure by Nocera was used, starting with 2,7-di-*tert*-butyl-4-bromo-5-iodo-9,9-dimethylxanthene.[4] ^{1}H NMR (d_6-DMSO, 300 MHz): δ 9.08 (s, 1H), 9.06 (s, 1H), 7.82 (s, 1H), 7.72-7.54 (m, 6H), 7.44-7.38 (m, 4H), 7.00-6.97 (m, 4H), 1.67 (s, 6H), 1.37 (s, 9H), 1.29 (s, 9H) ppm.

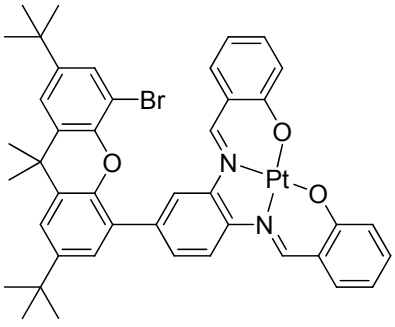

3: The procedure for **L2** was adopted using **L3**. ^{1}H NMR (CD_2Cl_2, 400 MHz): δ 9.05 (s, 1H), 8.94 (s, 1H), 8.48 (d, J = 1.2 Hz, 1H), 8.08 (d, J = 8.8 Hz, 1H), 7.66-7.61 (m, 3H), 7.57-6.56

(m, 2H), 7.54 (d, J = 1.8 Hz, 1H), 7.45-7.44 (m, 2H), 7.41 (d, J = 1.8 Hz, 1H), 7.24 (d, J = 8.8 Hz, 2H), 6.77 (m, 2H) ppm. Found: C, 57.05; H, 4.73; N, 3.13. Calc. for $C_{43}H_{41}N_2O_3BrPt$: C, 56.83; H, 4.55; N 3.08.

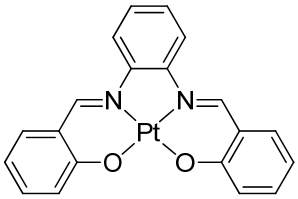

4: Modifications of a published procedure by Che was used.[5] ^{1}H NMR (d_6-DMSO, 300 MHz): δ 9.55 (s, 2H), 8.48-8.45 (m, 2H), 7.88 (dd, *J* = 8.1, 1.5 Hz, 2H), 7.58 (ddd, J = 8.7, 6.9, 1.8 Hz, 2H), 7.40 (m, 2H), 7.13 (d, *J* = 8.1 Hz, 2H), 6.80 (t, *J* = 8.1 Hz, 2H) ppm. Found: C,47.29; H, 3.00; N, 5.40. Calc. for $C_{20}H_{14}N_2O_2Pt$: C, 47.15; H, 2.77; N 5.50.

Table S1. Photophysical Data

Complex	λ_{max}/nm (ε/dm^3 mol^{-1} cm^{-1}) [a]	λ_{ex}/ nm	Fluid 298 K: [a] λ_{max}/nm (τ/μs); Φ	Fluid 77 K: [c] λ_{max}/nm (τ/μs)	Solid 298 K: λ_{max}/ nm (τ/μs)	Solid 77 K: λ_{max}/ nm (τ/μs)
1	259 (63210), 325 (36910), 366 (43020), 471 (9900), 535 (10550), 547 (10470)	546	635 (0.20); 0.007 [648 [b]]	650 (max; 7.0), 617, 705	668 (0.04)	679 (0.37)
2	260 (35510), 329 (26620), 371 (30120), 388 (29500), 454 (5950), 475 (6960), 537 (7220), 552 (7370)	555	635 (2.73); 0.08 [628 [b]]	613 (max; 8.20), 647, 748	659 (0.014)	665 (max; 1.06), 730 (0.62, 2.2)

[a] In CH_2Cl_2. [b] In CH_2Cl_2/CH_3CN (1:1). [c] In 2-Me-THF.

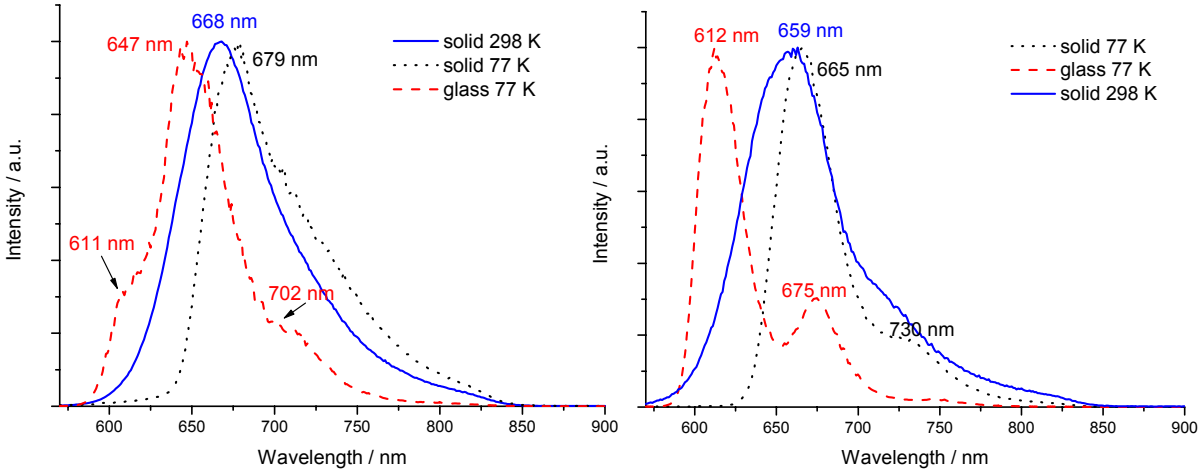

Figure S1. Left: Normalized emission spectra of **1** (left; 6.8×10^{-5} mol/L) and **2** (right; 4.2×10^{-5} mol/L) in solid state and 77 K glass.

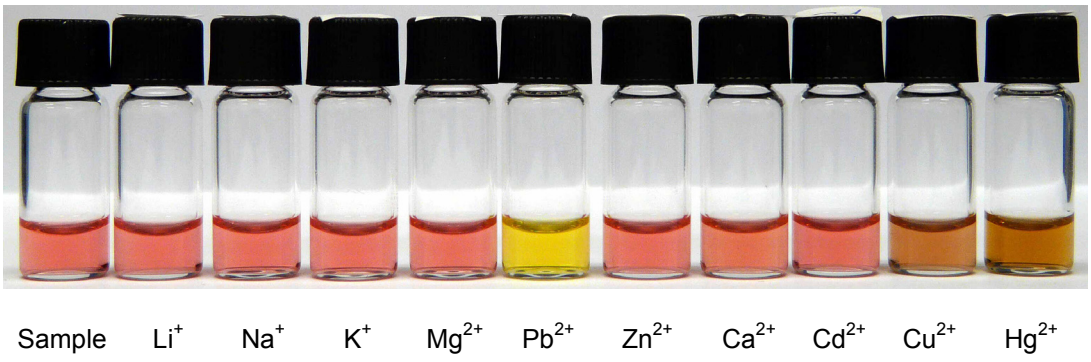

Figure S2. Colorimetric response of **1** (conc. = 6.4 × 10^{-5} mol/L) upon addition of 1 equivalent of M^{n+} in CH_3CN.

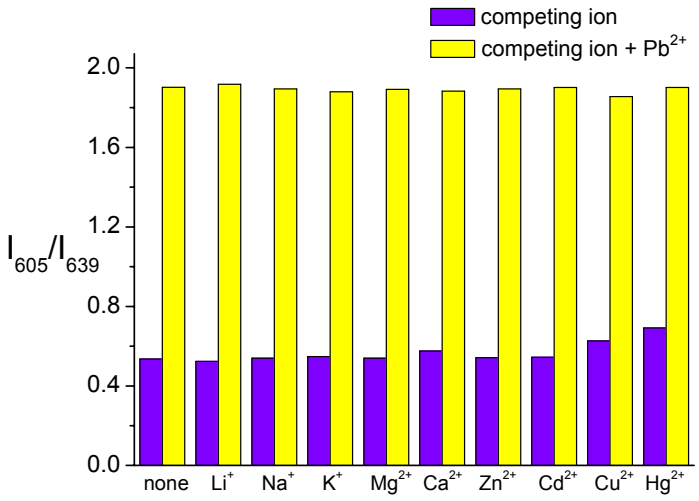

Figure S3. Competition experiments showing ratiometric phosphorescent response and selectivity of **1** for Pb^{2+} ions. The Pb^{2+} (1 equiv.) was added after solutions of **1** in CH_3CN (3.5 × 10^{-5} mol/L) had been incubated with 1 equivalent of metal ions. (λ_{ex} 501 nm)

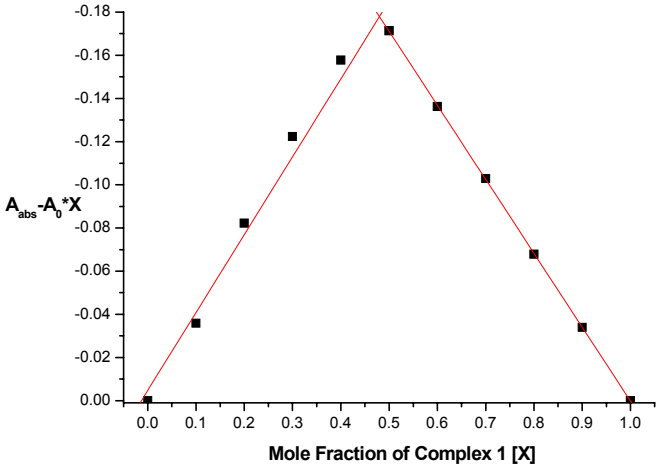

Figure S4. Job's plot of UV-vis data for Pb^{2+} binding by **1** in CH_3CN (concentration = 5.3×10^{-5} M), indicating 1:1 binding.

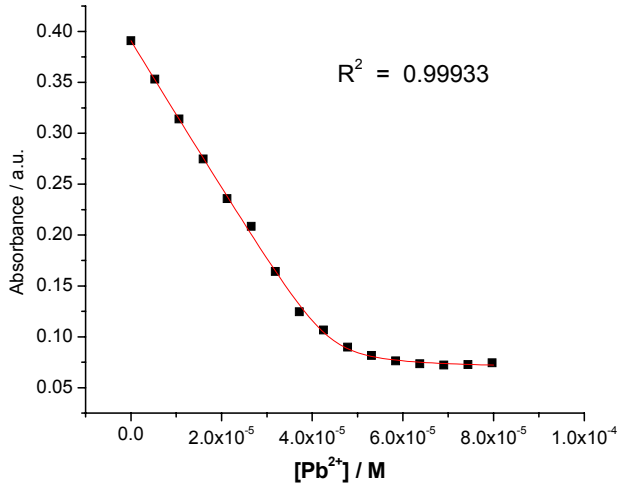

Figure S5. Absorbance at 534 nm as a function of Pb^{2+} concentration and its theoretical fit for the 1:1 binding of complex **1** with Pb^{2+}.[6] The log *K* was calculated to be 6.4 ± 0.1 in CH_3CN.

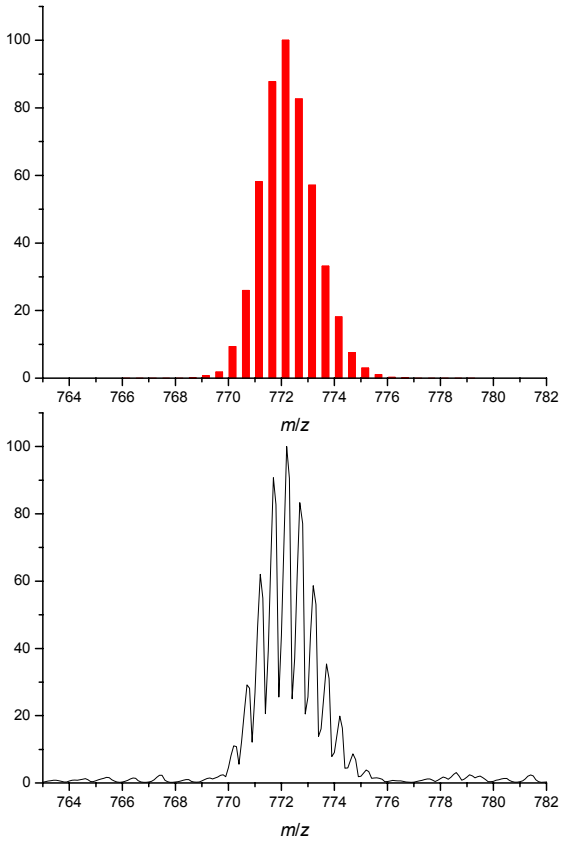

Figure S6. ESI-MS for 1:1 [**1** + Pb]$^{2+}$ species (m/z = 772.2) using declustering potential of 50 V in CH_3CN (top: calculated isotopic distribution with 0.5 amu separation between peaks). N.B. Cooperative 2:2 binding, which would afford 0.25 amu separations, can be disregarded (additional evidence: non-sigmoidal binding curve gives excellent fit for 1:1 binding; Hill plot does not show positive cooperation).

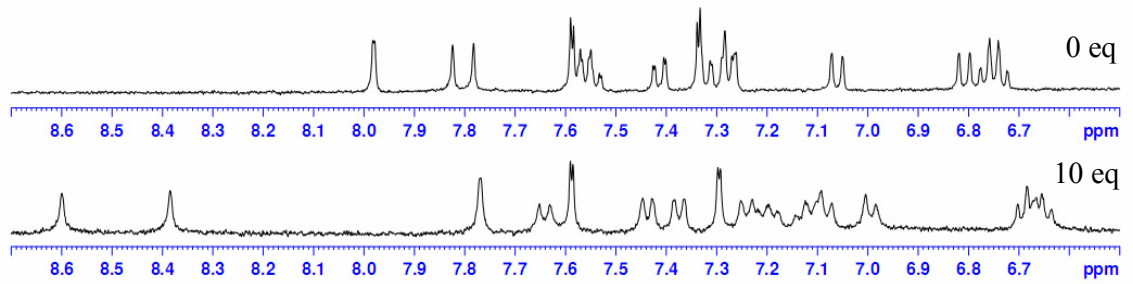

Figure S7. ^{1}H NMR spectra (400 MHz) of **1** before and after addition of $Pb(ClO_4)_2$ in CD_2Cl_2/CD_3CN (3:1). The ^{1}H NMR shift differences between each side of the non-symmetric salphen fragment become greater with added Pb^{2+} ions, indicating increased rigidity within **1**, while the downfield perturbations are consistent with decreased ring currents and thus greater separation of salphen units (see Scheme S1).

Emission Changes of 1–4 with Pb^{2+}

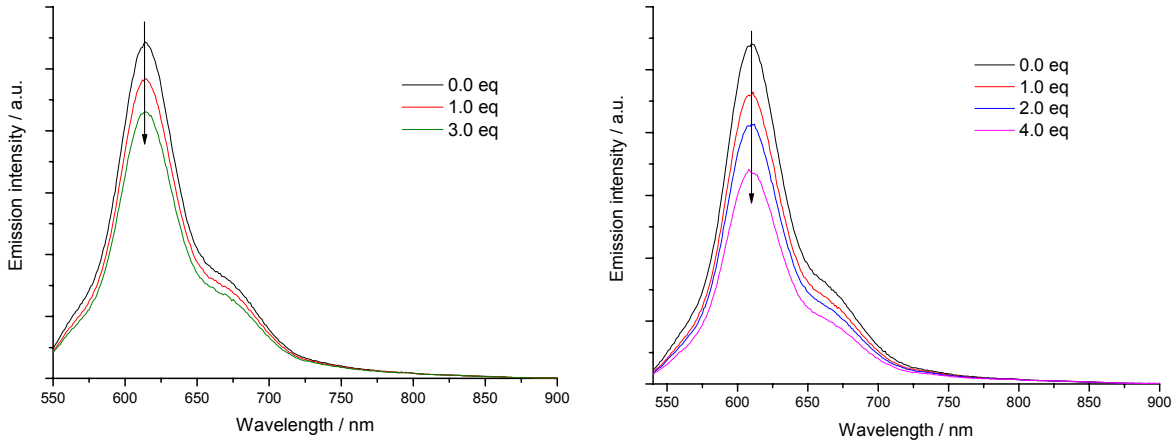

Figure S8. Emission quenching of **3** (left) and **4** (right) (both 5×10^{-5} M in CH_3CN; λ_{ex} 530 nm) upon addition of Pb^{2+}.

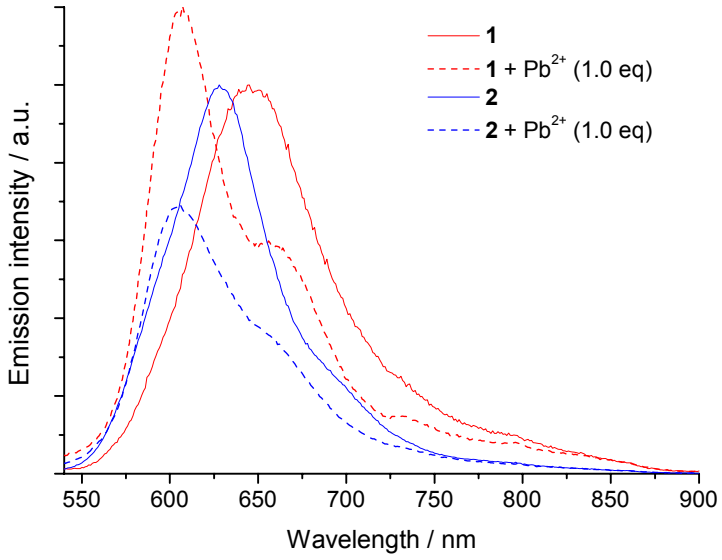

Figure S9. Emission spectra of **1** and **2** (normalized, 2×10^{-5} M, λ_{ex} 501 nm) in CH_3CN/CH_2Cl_2 (1/1), and relative changes upon addition of Pb^{2+} (1 equiv.).

Calculated Structure of 1

Complex **1** was optimized using DFT (hybrid Hartree-Fock DFT functional B3LYP level, which is a combination of the Becke 3-parameter exchange and Lee-Yang-Parr correlation functional, using the Gaussian 03 program package) with the CEP-31G basis set. In the energy-minimized calculated structure, which was confirmed to be a minimum from vibrational frequency calculations, intramolecular 'offset π-stacked' interplanar contacts of around 3.5-3.6 Å are apparent within the $(Pt\text{-salphen})_2$ moiety (see Scheme S1).

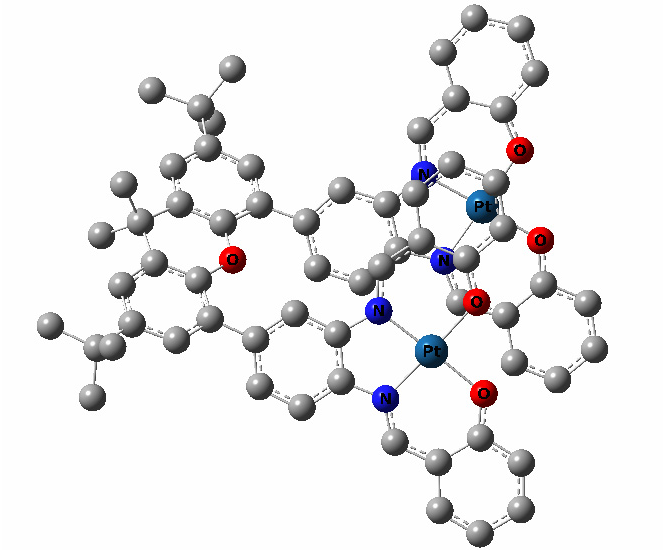

Figure S10. Perspective views of energy-minimized calculated structure of **1**.

The O_4-binding structure for $[\mathbf{1}\cdot Pb\cdot ClO_4]^+$ was similarly optimized. In the energy-minimized structure, which was confirmed to be a minimum from vibrational frequency calculations, the Pb^{2+} ion sits in the center of the 4 oxygen donors and is bound by a bidentate perchlorate group, while the Pt-salphen planes are more distorted and separated compared to those in Figure S10 (see Scheme S1).

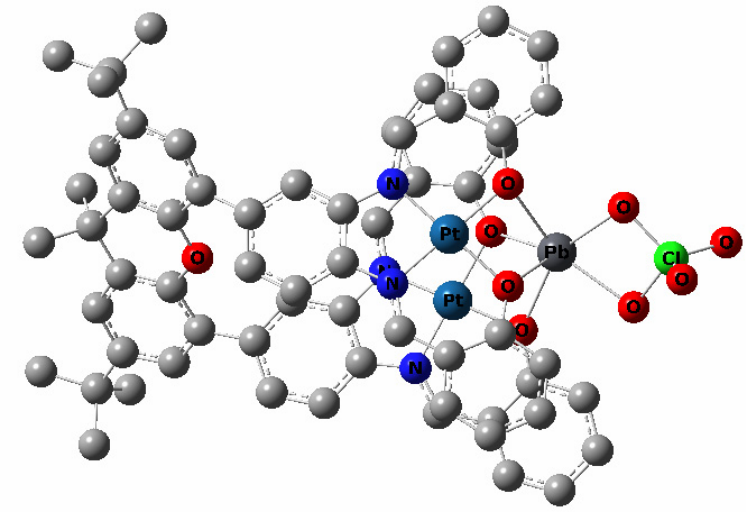

Figure S11. Perspective views of energy-minimized calculated structure of $[\mathbf{1}\cdot Pb\cdot ClO_4]^+$.

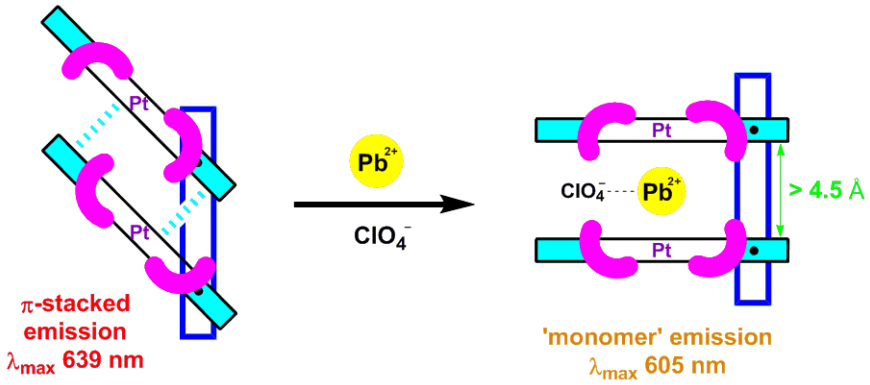

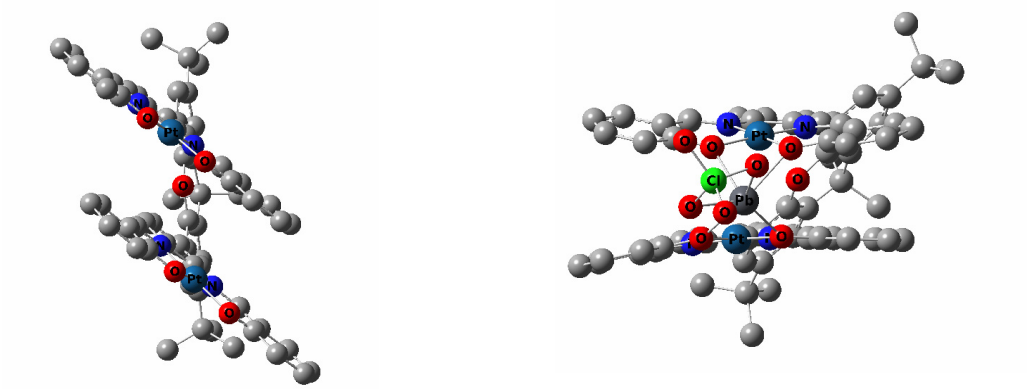

Carbonaro *et al.*:

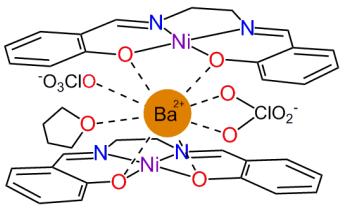

PScheme S1. Top: Schematic representation of possible mechanism for Pb^{2+} binding by **1** ("C" represent potential O donors on salphen). Center: 'Head-on' views of the energy-minimized calculated structures of **1** and $[\mathbf{1}\cdot Pb\cdot ClO_4]^+$. Bottom: An illustration of the related X-ray crystal structure of $[\{Ni(salen)\}_2Ba(ClO_4)_2(thf)]$, featuring two mononuclear Ni(salen) acting as bidentate moieties, one mono- and one bidentate perchlorate groups, and one thf ligand completing the coordination sphere around Ba^{2+}.[7]

Similarities between (a) the schematic diagram and calculated structures, with regards to the positions of the O donor atoms, and (b) the $[\{Ni(salen)\}_2Ba(ClO_4)_2(thf)]$ and calculated $[\mathbf{1}\cdot Pb\cdot ClO_4]^+$ structures, are apparent.

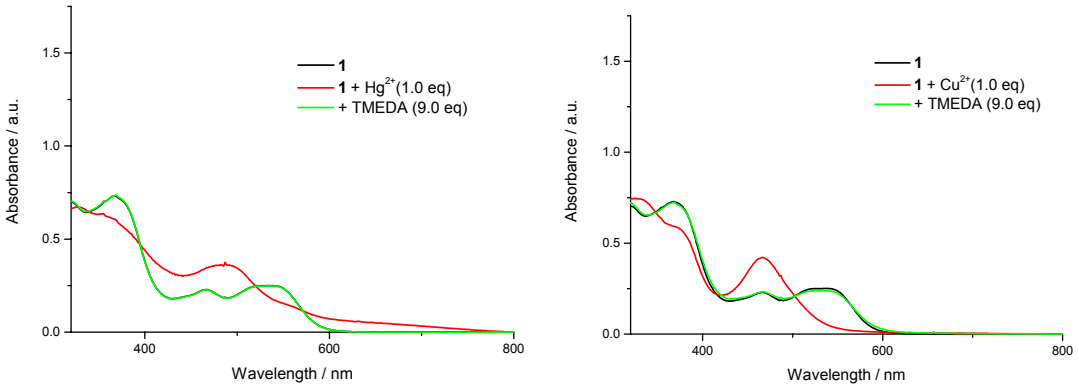

Figure S12. The reversibility of the response of **1** to Hg^{2+} and Cu^{2+} has been studied by the following UV-vis experiments in CH_3CN at 298 K. Upon addition of 1 equiv. of Hg^{2+} (left), a blue shift for the lowest energy absorption band was observed. Subsequent addition of TMEDA (9 equiv.), acting as Hg^{2+} scavenger, caused the absorption spectrum to revert back to the original. This indicates that the reaction of **1** with Hg^{2+} in CH_3CN is reversible. Comparable results are obtained for Cu^{2+} (right).

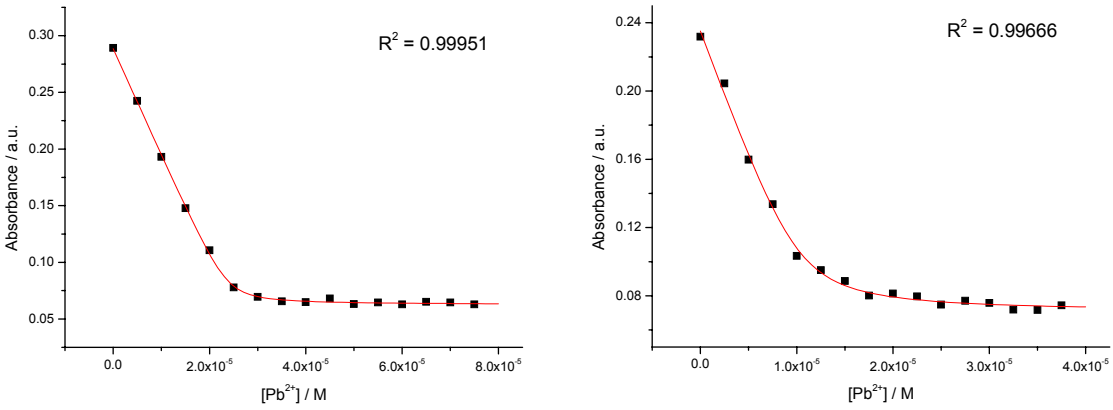

Figure S13. Absorbance at 534 nm as a function of Pb^{2+} concentration and its theoretical fit for the 1:1 binding of complex **1** (left) and **2** (right) with Pb^{2+} in CH_3CN/CH_2Cl_2 (1/1); the log *K* was calculated to be 6.63 ± 0.06 and 6.20 ± 0.15 respectively, indicating weaker binding by **2**.

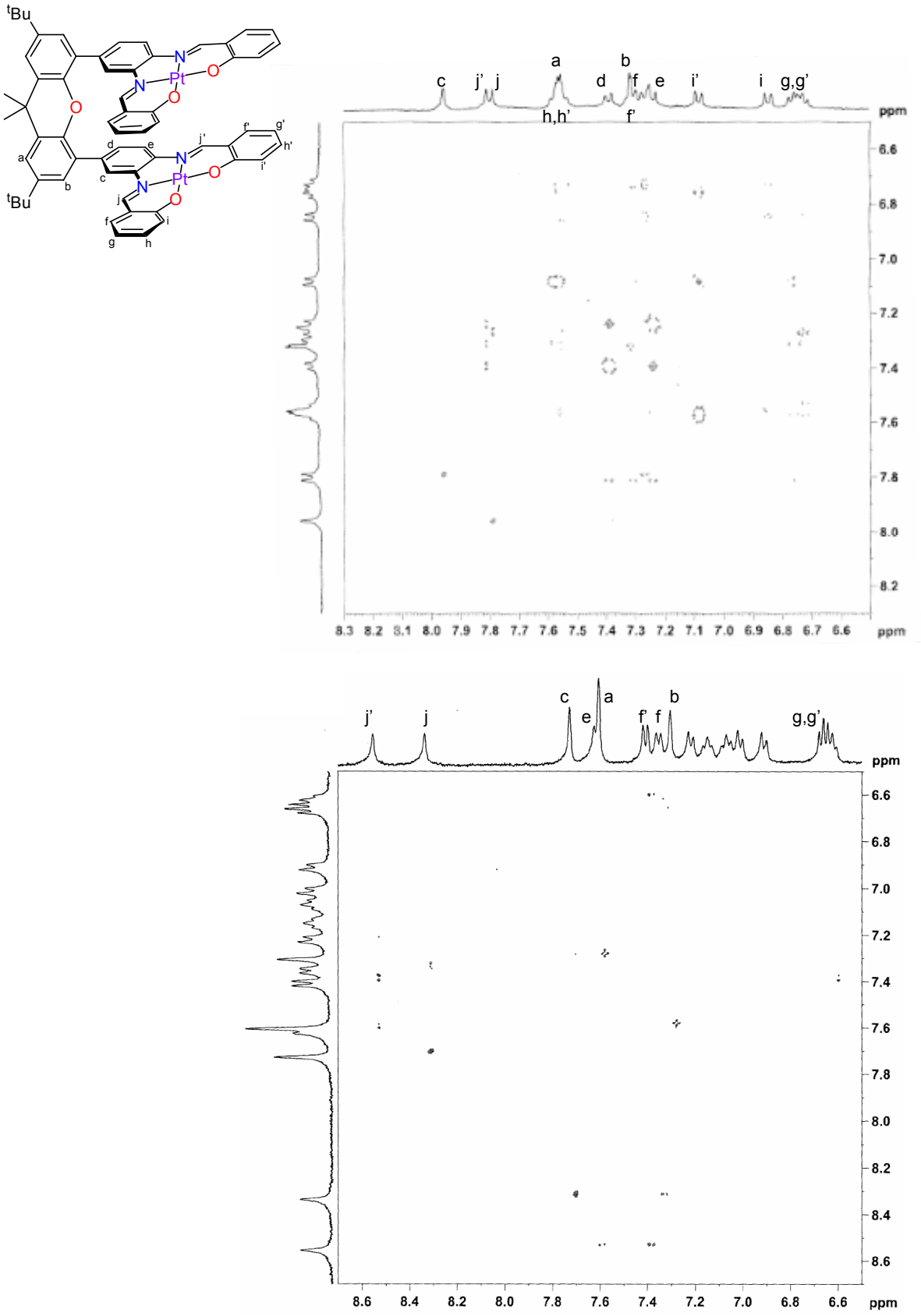

Figure S14. $^{1}H,^{1}H$ ROESY NMR spectra (400 MHz) of **1** before [top; CD_2Cl_2/d_6-DMSO (9:1)] and after [bottom; CD_2Cl_2/CD_3CN (3:1)] addition of $Pb(ClO_4)_2$.

ESI References

1 J. N. Demas and G. A. Crosby, *J. Phys. Chem.,* 1971, **75**, 991.

2 R. Okamura, T. Wada, K. Aikawa, T. Nagata and K. Tanaka, *Inorg. Chem*., 2004, **43**, 7210.

3 E. B. Schwartz, C. B. Knobler and D. J. Cram, *J. Am. Chem. Soc*., 1992, **114**, 10775.

4 S.-Y. Liu and D. G. Nocera, *J. Am. Chem. Soc*., 2005, **127**, 5278.

5 C.-M. Che, S.-C. Chan, H.-F. Xiang, M. C. W. Chan, Y. Liu and Y. Wang, *Chem. Commun.,* 2004, 1484.

6 J. Bourson, J. Pouget and B. Valeur, *J. Phys. Chem.,* 1993, **97**, 4552.

7 L. Carbonaro, M. Isola, P. La Pegna, L. Senatore and F. Marchetti, *Inorg. Chem.,* 1999, **38**, 5519.